THE JOURNAL OF BIOLOGICAL CHEMISTRY VOL. 281, NO. 52, pp. 39881–39890, December 29, 2006

Cysteine-scanning Analysis of the Nucleobase-Ascorbate Transporter Signature Motif in YgfO Permease of *Escherichia coli*

*Gln-324 AND Asn-325 ARE ESSENTIAL, AND Ile-329–Val-339 FORM AN α-HELIX**[S]

Received for publication, June 15, 2006, and in revised form, September 27, 2006 Published, JBC Papers in Press, October 31, 2006, DOI 10.1074/jbc.M605748200

Panayiota Karatza, Panayiotis Panos, Ekaterini Georgopoulou, and Stathis Frillingos[1]

From the Laboratory of Biological Chemistry, University of Ioannina Medical School, 45110 Ioannina, Greece

The nucleobase-ascorbate transporter (NAT) signature motif is a conserved sequence motif of the ubiquitous NAT/NCS2 family implicated in defining the function and selectivity of purine translocation pathway in the major fungal homolog UapA. To analyze the role of NAT motif more systematically, we employed Cys-scanning mutagenesis of the *Escherichia coli* xanthine-specific homolog YgfO. Using a functional mutant devoid of Cys residues (C-less), each amino acid residue in sequence ^{315}GSIPITTFAQNNGVIQMTGVASRYVG^{340} (motif underlined) was replaced individually with Cys. Of the 26 single-Cys mutants, 16 accumulate xanthine to ≥50% of the steady state observed with C-less YgfO, 4 accumulate to low levels (10–25% of C-less), F322C, N325C, and N326C accumulate marginally (5–8% of C-less), and P318C, Q324C, and G340C are inactive. When transferred to wild type, F322C(wt) and N326C(wt) are highly active, but P318G(wt), Q324C(wt), N325C(wt), and G340C(wt) are inactive, and G340A(wt) displays low activity. Immunoblot analysis shows that replacements at Pro-318 or Gly-340 are associated with low or negligible expression in the membrane. More extensive mutagenesis reveals that Gln-324 is critical for high affinity uptake and ligand recognition, and Asn-325 is irreplaceable for active xanthine transport, whereas Thr-332 and Gly-333 are important determinants of ligand specificity. All single-Cys mutants react with *N*-ethylmaleimide, but regarding sensitivity to inactivation, they fall to three regions; positions 315–322 are insensitive to *N*-ethylmaleimide, with IC_{50} values ≥0.4 mM, positions 323–329 are highly sensitive, with IC_{50} values of 15–80 μM, and sensitivity of positions 330–340 follows a periodicity, with mutants sensitive to inactivation clustering on one face of an α-helix.

The nucleobase-ascorbate transporter (NAT)[2] or nucleobase-cation symporter-2 (NCS2) family is an evolutionarily ubiquitous family of purine, pyrimidine, and L-ascorbate transporters, with members specific for the cellular uptake of uracil, xanthine or uric acid (microbial and plant genomes), or vitamin C (mammalian genomes) (1–3). Despite their importance as molecular gateways for the recognition and uptake of several frontline purine-related drugs, NAT/NCS2 members have not been studied systematically at the molecular level, and high resolution structures or mechanistic models are missing. More than 500 sequence entries are known, but few are functionally characterized in detail.

The first NAT to be sequenced and most extensively studied thus far is UapA, a high affinity uric acid/xanthine:H^+ symporter from the ascomycete *Aspergillus nidulans* (4). The *A. nidulans* genome encodes two well characterized NAT proteins, UapA and UapC, which are uric acid-xanthine (purine) transporters, with similar but distinct kinetic and physiological characteristics. Chimeric purine transporter analysis between UapA and UapC coupled with site-directed mutagenesis and second-site suppressor analysis of selected UapA mutants (5–8) have defined a conserved NAT/NCS2-motif region that includes residues affecting substrate recognition and selectivity. This conserved sequence region is located between putative transmembrane helices (TMHs) 8 and 9 and immediately downstream of a putative α-helical amphipathic region of ambiguous topology. It includes the consensus sequence (Q/E/P)**N***X***G***XXXX***T**(R/K/G) that was designated as the NAT signature motif (5). Further molecular genetic and biochemical evidence led the authors to propose that at least one residue of the NAT motif, Gln-408, is implicated in binding with the imidazole ring of purines (8) either indirectly through transmission of conformational changes or directly. In addition, based on second-site suppressor and mutational analysis, a residue at the middle of putative TMH12 (Phe-528) was proposed to act as a substrate-selectivity filter to determine stringency of the purine translocation pathway (7, 9).

Recently, we have cloned and characterized the first purine-specific members of the NAT/NCS2 family from a Gram-neg-

* This research was co-funded by the European Union in the framework of the program Heraklitos of the Operational Program for Education and Initial Vocational Training of the 3rd Community Support Framework of the Hellenic Ministry of Education, funded by 25% from national sources and by 75% from the European Social Fund. The costs of publication of this article were defrayed in part by the payment of page charges. This article must therefore be hereby marked "*advertisement*" in accordance with 18 U.S.C. Section 1734 solely to indicate this fact.

[S] The on-line version of this article (available at http://www.jbc.org) contains supplemental Figs. S1–S3 and Tables S1 and S2.

[1] To whom correspondence should be addressed. Tel.: 30-26510-97814; Fax: 30-26510-97868; E-mail: efriligo@cc.uoi.gr.

[2] The abbreviations used are: NAT, nucleobase-ascorbate transporter; NCS2, nucleobase-cation symporter-2; TMH, transmembrane helix; IPTG, isopropyl 1-thio-β-D-galactopyranoside; Cys-less (C-less), permease devoid of native Cys residues; OGM, Oregon green 488 maleimide; HRP, horseradish peroxidase; BAD, biotin-acceptor domain; NEM, *N*-ethylmaleimide.

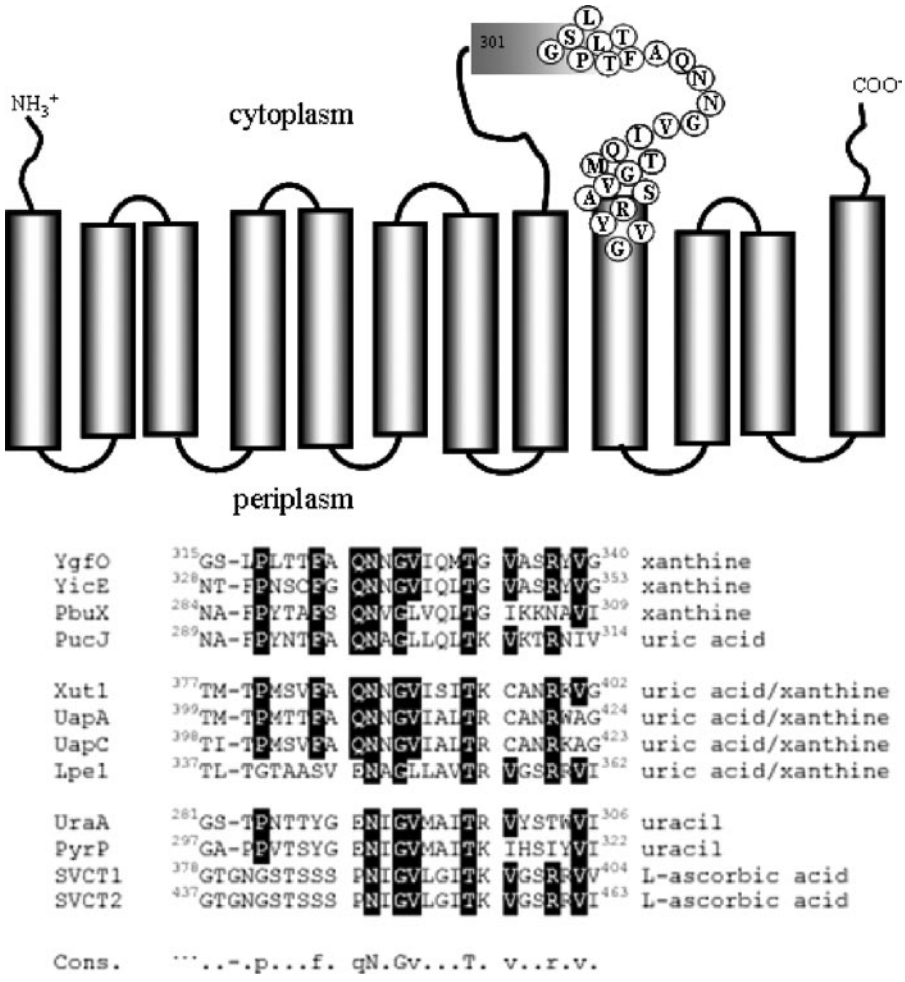

FIGURE 1. **Proposed topology and sequence alignment of the NAT motif and flanking regions of YgfO.** The topology diagram (*upper panel*) illustrates the location of sequence 315–340 in the context of the overall topological organization of YgfO. The model is based on program TMHMM, evidence that C terminus is cytoplasmic (25) and our unpublished evidence[3] on the orientation of TMHs 8–12. The sequence alignment (*lower panel*) shows a consensus of the 12 characterized NAT/NCS2 transporters, including *E. coli* YgfO (AAC75920) (10), YicE (AAC76678), and UraA (AAC75550), *Bacillus subtilis* PbuX (CAB14123) and PucJ (CAB15233), *Lactococcus lactis* PyrP (AAK05701), *A. nidulans* UapA (X71807) (8) and UapC (P487777), *Candida albicans* Xut1 (AAX2221) (11), *Zea mays* Lpe1 (AAB17501) (31), and *Homo sapiens* SVCT1 (AAH50261) and SVCT2 (CAC16126). The sequences were aligned using ClustalW. Residues similar to the consensus (*Cons.*) are *shaded*, and conservative substitutions are shown in *lowercase*.

ative bacterium, namely YgfO and YicE of *Escherichia coli* K-12 (10). Both proteins were shown to function as specific, high affinity xanthine:H^+ symporters that cannot use uric acid, hypoxanthine, uracil, or other nucleobases as a substrate and cannot recognize analogues substituted at positions 7 or 8 of the imidazole ring (10, 11). We have shown that YgfO in particular can be expressed at high levels in the inner membrane of *E. coli* K-12 under control of a plasmid-borne, IPTG-inducible promoter system (10). YgfO can also be tagged at its C terminus with a number of different immunodetection and affinity-purification epitopes without affecting the xanthine uptake activity (10). Because analytical evidence on the topology, tertiary structure, binding site, or mechanism of the nucleobase:cation symport is still missing for any NAT, we have taken advantage of the *E. coli* system to employ Cys-scanning mutagenesis, a strategy that has addressed these problems in many other transport proteins (12–18). A fully functional version, equivalent to wild-type YgfO, has been constructed, in which all five native Cys residues have been replaced with Ser (Cys-less YgfO).[3] On the basis of the Cys-less background, we have initiated an ongoing, systematic series of Cys-scanning and site-directed mutagenesis studies to elucidate structure-function relationships in a bacterial NAT.

One of the first issues to be addressed is to analyze the NAT-signature motif and define whether it contains side chain determinants that consent and/or differentiate between a bacterial and a fungal homolog (Fig. 1). In this vein, we have performed a systematic Cys-scanning and site-directed mutagenesis study of sequence 315–340 that includes the NAT-signature motif (residues 324–333) and flanking regions of the transporter. Our combined biochemical evidence from transport, immunoblotting, sulfhydryl alkylation, and ligand-inhibition assays of a set of 50 site-directed permease mutants has led to an initial model of the secondary structure and topology in this region and indicated few residues that are critical for the operation of a functional YgfO transporter. The significance of our findings with respect to comparison with the major fungal NAT homolog (UapA) is discussed.

EXPERIMENTAL PROCEDURES

Materials—[8-^{3}H]Xanthine (27.6 Ci/mmol) was purchased from Moravek Biochemicals. Nonradioactive nucleobases and analogues were from Sigma. Oregon green 488 maleimide (OGM) was from Molecular Probes. Pro-Bond resin was from Invitrogen. Oligodeoxynucleotides were synthesized from BioSpring GmbH. High fidelity Taq polymerase (Expand High Fidelity PCR system) was from Roche Applied Science. Site-directed rabbit polyclonal antiserum against the C-terminal 12 peptides of *E. coli* LacY was donated by H. R. Kaback (UCLA) and prepared by Berkeley Antibody Co., Inc. Horseradish peroxidase (HRP)-conjugated penta-His antibody was from Qiagen, and polyclonal anti-OGM antibody was from Molecular Probes. Avidin-HRP and protein A-HRP conjugates were from Amersham Biosciences. All other materials were reagent grade and obtained from commercial sources.

Bacterial Strains and Plasmids—*E. coli* K-12 was transformed according to Inoue (19). TOP10F′ (Invitrogen) was

[3] P. Karatza, E. Georgopoulou, and S. Frillingos, manuscript in preparation.

used for initial propagation of recombinant plasmids. T184 (20) harboring pT7-5/*ygfO* (10) with given replacements was used for IPTG-inducible expression from the *lacZ* promoter/operator (p/o).

DNA Manipulations—Construction of expression plasmids and BAD-tagged versions of YgfO containing a C-terminal tail with the biotin-acceptor (BAD) domain of *Klebsiella pneumoniae* oxaloacetate decarboxylase and the C-terminal 12 peptides of *E. coli* LacY has been described (10). For construction of His_{10}-tagged versions, the coding sequence of *ygfO* was PCR-amplified from pT7-5/*ygfO* using antisense primers with non-annealing 5′ overhangs containing an ApaI site and transferred in pT7-5/*lacY(C154G)*-His_{10} (21) by BamHI-ApaI restriction fragment replacement; the resulting constructs contain the C-terminal 12 peptides of *E. coli* LacY followed in-frame by 10 His residues and a stop codon.

For construction of Cys-less YgfO, the five native-Cys codons were replaced simultaneously with Ser codons using two-stage (multiple overlap/extension) PCR on the template of wild-type YgfO tagged at C terminus with the BAD tag. Details of this procedure will be published separately.[3] Cys-less YgfO was also transferred to the His_{10}-tagged background by BamHI-HpaI restriction fragment replacement. For construction of Cys replacement mutants, two-stage (overlap/extension) PCR (22) was performed on the template of Cys-less YgfO tagged at the C terminus with either BAD or His_{10} as indicated. The entire coding sequence of all engineered constructs was verified by double-strand DNA sequencing in an automated DNA sequencer (MWG-Biotech).

Growth of Bacteria—E. coli , harboring given plasmids, was grown aerobically at 37 °C in Luria-Bertani medium containing streptomycin (0.01 mg/ml) and ampicillin (0.1 mg/ml). Fully grown cultures were diluted 10-fold, allowed to grow to mid-logarithmic phase, induced with IPTG (0.5 mM) for an additional 2 h at 37 °C, harvested, and washed with the appropriate buffers.

Transport Assays and Kinetic Analysis—E. coli T184 were assayed for active transport of [^{3}H]xanthine (1 μM) by rapid filtration at both 25 °C and 37 °C as described (10). For assaying the effect of *N*-ethylmaleimide (NEM), T184 cells were preincubated with NEM at the indicated conditions, reactions were stopped by the addition of a 20-fold excess of dithiothreitol, and transport assays were performed in the presence of phenazine methosulfate (0.2 mM), and potassium ascorbate (20 mM) (23).

For ligand competition experiments, uptake of [^{3}H]xanthine (1 μM) was first assayed in the absence or presence of unlabeled analogues (1 mM) that had been pre-equilibrated in the assay mixture for 5 min. For kinetic analysis, putative inhibitors were used in the concentration range of 0.1 μM to 1.5 mM, and data were fitted to the appropriate equations using *Prism*4. IC_{50} values were determined from full dose-response curves with a minimum of eight points spread over the relevant range. In all cases the Hill coefficient was close to -1, consistent with presence of one binding site. In addition, we have examined the effect of two analogues (1-methyl and 8-methylxanthine) on K_m and V_{max} for wild-type and selected mutants and showed that V_{max} remains unaltered, consistent with competitive inhibition (supplemental Fig. S2 and Table S2). This evidence suggests that a simple model of competition with the binding site of the transporter is applicable, satisfying the criteria for use of the Cheng and Prusoff equation $K_i = IC_{50}/(1 + (L/K_m))$ (where L is the permeant concentration, and K_m is the value obtained for this permeant) (11). It should be noted that the K_i value is an affinity constant implying binding to the transporter but does not indicate whether the ligand is being transported across the membrane.

Immunoblot Analysis—Membrane fractions of *E. coli* T184 harboring given plasmids were prepared and subjected to SDS-PAGE (12%) as described (10). Proteins were electroblotted to polyvinylidene difluoride membranes (Immobilon-PVDF; Pall Corp.). YgfO-BAD was probed with avidin-HRP or with a polyclonal antibody against the C terminus of *E. coli* LacY (24) followed by protein A-HRP. YgfO-His_{10} was probed with penta-His antibody-HRP. Signals were developed with enhanced chemiluminescence (ECL).

Sulfhydryl Alkylation Assay—E. coli T184 expressing His_{10}-tagged versions of the indicated permeases were harvested, washed twice in Tris-NaCl buffer (50 mM Tris, pH 7.5, 100 mM NaCl), normalized to an A_{420} of 3.0 (0.2 mg of total protein/ml), and incubated for 10 min at 25 °C in the absence or presence of NEM (1 mM) followed by washing in Tris-NaCl buffer containing 1 mM Pefabloc (Sigma), preparation of membrane fractions, resuspension in Tris-NaCl buffer (100 μl), and extraction of the membrane proteins with *n*-dodecyl-β-D-maltoside (0.8% w/v) for 15 min at room temperature. The protein extract was then diluted to 400 μl and mixed with Ni^{2+}-IDA beads (ProBond resin) (50 μl) that had been pre-equilibrated in Tris-NaCl buffer containing 0.08% (w/v) *n*-dodecyl-β-D-maltoside and 30 mM imidazole and incubated for 1 h at room temperature with rotation. After incubation, the beads were washed with 40 volumes of denaturation buffer (Tris-NaCl buffer containing 6 M urea and 0.5%, w/v, SDS), resuspended in 0.1 ml of the same buffer containing OGM (0.2 mM), and incubated for 20 min with rotation at room temperature. The OGM reaction was stopped with the addition of dithiothreitol (5 mM), and the Ni^{2+}-IDA beads were pelleted and resuspended in Laemmli buffer containing 0.07 M Na_2EDTA at 30 °C for 10 min before SDS-PAGE (12%) and immunoblotting. Protein concentrations were determined with the micro-BCA method (Pierce).

In Silico Analysis—Comparative sequence analysis of NAT/NCS2 homologs was based on BLAST-p search and ClustalW alignment; the most recent genome annotations were used for retrieving sequence data. Analysis of transmembrane topology was performed using program TMHMM (25).

RESULTS

Active Xanthine Transport—Using a functional YgfO devoid of Cys residues (C-less), each amino acid residue in sequence ^{315}GSIPITTFA**QN**N**G**VIQM**TG**VASRYVG^{340} including the NAT motif (in underlined boldface) was replaced individually with Cys. After verification of the sequence, each single-Cys mutant was transformed into *E. coli* T184 and assayed for its ability to catalyze active xanthine transport. As shown in Fig. 2*A*, of the 26 single-Cys mutants, 10 transport xanthine at rates that are between 75 and 100% or more of C-less permease, and an additional 5 mutants transport at rates that are between 40

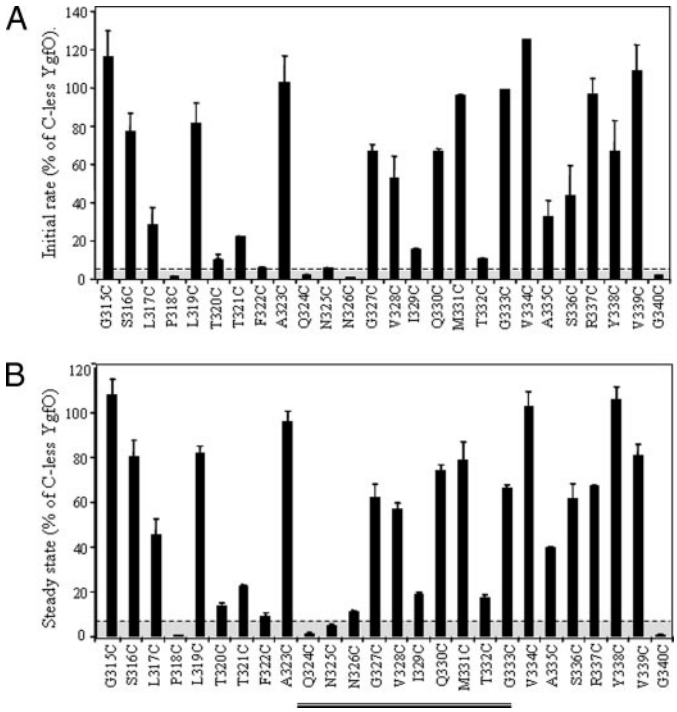

FIGURE 2. **Active xanthine transport activities of single-Cys mutants.** *E. coli* T184 harboring pT7-5/*ygfO*(C-less-BAD) with given mutations were grown aerobically at 37 °C in complete medium to mid-logarithmic phase, induced with IPTG (0.5 mM) for 2 h, normalized to 0.7 mg of protein/ml of cell suspension, and assayed for transport of [^{3}H]xanthine (1 μM) at 25 °C. *A*, initial rates of uptake measured at 5–20 s. Control values obtained from T184 harboring pT7-5 alone (0.02 nmol mg^{-1} min^{-1} on average) were subtracted from the sample measurements in all cases. Results are expressed as a percentage of the rate of Cys-less YgfO (1.7 nmol mg^{-1} min^{-1} on average) with S.D. from three independent determinations. *B*, steady state levels of xanthine accumulation (reached at 1–10 min for most mutants). Control values obtained from T184 harboring pT7-5 alone (0.01 nmol mg^{-1} on average) were subtracted from the sample measurements in all cases. Results are expressed as a percentage of the level of Cys-less YgfO (0.8 nmol mg^{-1} on average) with S.D. from three independent determinations. The motif sequence 324–333 is *double-underlined*.

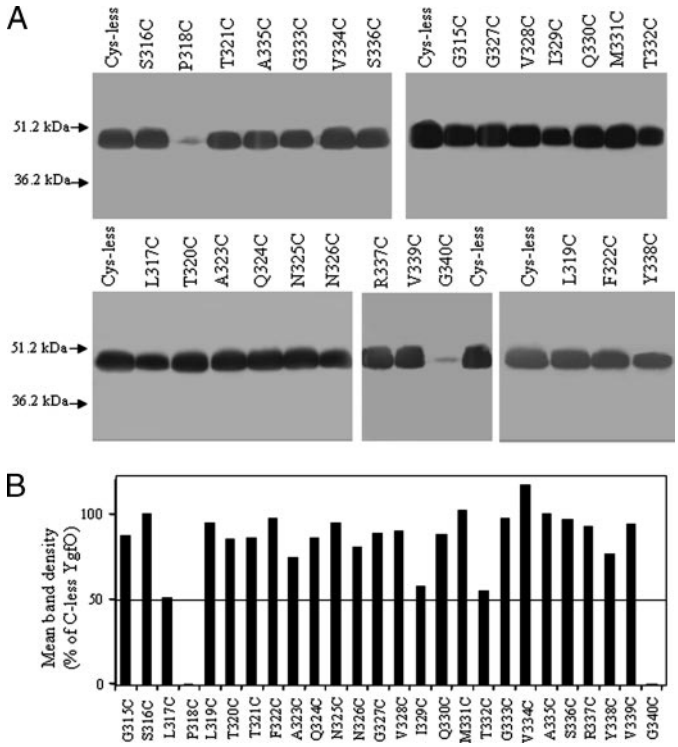

FIGURE 3. **Immunoblot analysis of single-Cys mutants.** Membranes were prepared from IPTG-induced cultures of *E. coli* T184 harboring pT7-5/*ygfO*(C-less-BAD) with given mutations. Samples containing ~100 μg of membrane protein were subjected to SDS-PAGE (12%) and immunoblotting using HRP-conjugated avidin. Equivalent results were obtained when blots were re-probed with anti-LacY epitope antibody (not shown). *A*, representative blots of single-Cys mutants and Cys-less YgfO. Membranes prepared from cells harboring pT7-5 alone exhibited no immunoreactive material. Prestained molecular weight standards (Bio-Rad, low range) are shown on the *left*. *B*, quantitative estimation of the expression level of each mutant as a percentage of Cys-less expression derived from the relative density of the corresponding band. Results shown are the means of four determinations from two independent experiments, with S.D. that were <15%.

and 60% of C-less. Five mutants (L317C, T320C, T321C, I329C, and T332C) display low but significant uptake rates (10–25% of C-less). Finally, mutants P318C, F322C, Q324C, N325C, N326C, and G340C display rates that approximate cells transformed with vector containing no *ygfO* insert. Steady state levels of xanthine accumulation also show the same general picture (Fig. 2*B*); of the 26 single-Cys mutants, 14 accumulate xanthine to >60% of the steady state observed with C-less YgfO, and an additional 2 exhibit levels of 40–50%. Of the remaining 10 mutants, T320C, T321C, I329C, and T332C exhibit low levels of accumulation (10–25% of C-less), F322C, N325C, and N326C accumulate marginally (5–8% of C-less), whereas P318C, Q324C, and G340C are completely inactive. Similar findings were obtained with the single-Cys mutants in either the BAD-tagged or the His_{10}-tagged permease background (Fig. 2 and data not shown).

Expression in the Membrane—Immunoblot analysis of BAD-tagged single-Cys permeases shows that negligible activity of mutants P318C and G340C is because of negligible expression in the membrane. All other mutants are expressed to high or moderate levels (Fig. 3). The compromised expression (~50% of C-less) displayed by mutants L317C, I329C, and T332C reflects their low transport rates (23, 11, and 9% of C-less) that are disproportional to their much higher levels of accumulation (46, 18, and 15% of C-less, respectively) (Fig. 2). Qualitatively similar data were obtained with the set of single-Cys mutants in the His_{10}-tagged permease background (not shown).

Expression and Transport Analysis of Mutants in Wild-type Background—From the Cys-scanning transport analysis described above, few positions of inactive or marginally active mutants were delineated. We analyzed these positions further by (*a*) transferring single-Cys mutations to the wild-type YgfO background and/or (*b*) engineering the most conservative site-directed replacement mutant to introduce an amino acid other than Cys. Thus, we constructed and assayed mutants (*a*) F322C(wt), Q324C(wt), N325C(wt), N326C(wt), and G340C(wt) and (*b*) P318G(wt), Q324N(wt), N325Q(wt), N326Q(wt), and G340A(wt) (Fig. 4). We found that F322C(wt), N326C(wt), and N326Q(wt) were highly active, G340A(wt) accumulated to 50% of wild type, Q324N(wt), N325C(wt), and N325Q(wt) accumulated to very low levels (10–25% of wild type), whereas P318G(wt), Q324C(wt), and G340C(wt) were completely inactive (Fig. 4, *B* and *C*). Negligible activity of P318G(wt) or G340C(wt) is corroborated by low or negligible expression in the membrane, and the relatively low activity of

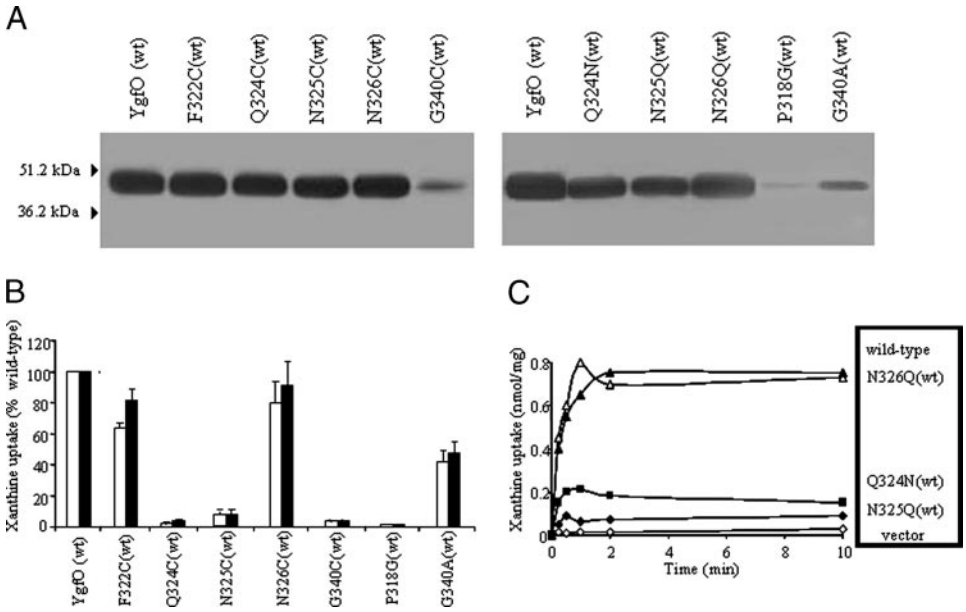

FIGURE 4. **Expression and xanthine uptake activities of Cys-replacement and most-conservative-replacement mutants in the wild-type permease background.** *E. coli* T184 harboring pT7-5/*ygfO*(wild-type-BAD) with given mutations were grown, induced, and subjected to immunoblot analysis of membrane fractions (*A*) or assayed for transport of [^{3}H]xanthine (1 μM, 25 °C) (*B* and *C*) exactly as described in the legends to Figs. 2 and 3. *Open* and *closed histogram bars* in *panel B* represent initial rate and steady state values, respectively, with S.D. shown from three independent experiments. *C*, representative time courses of xanthine transport by mutants Q324N(wt) (*filled rectangles*), N325Q(wt) (*filled rhombuses*). and N326Q(wt) (*filled triangles*) in comparison with wild-type YgfO (*open triangles*) and negative controls (cells harboring vector pT7-5 alone) (*open rhombuses*).

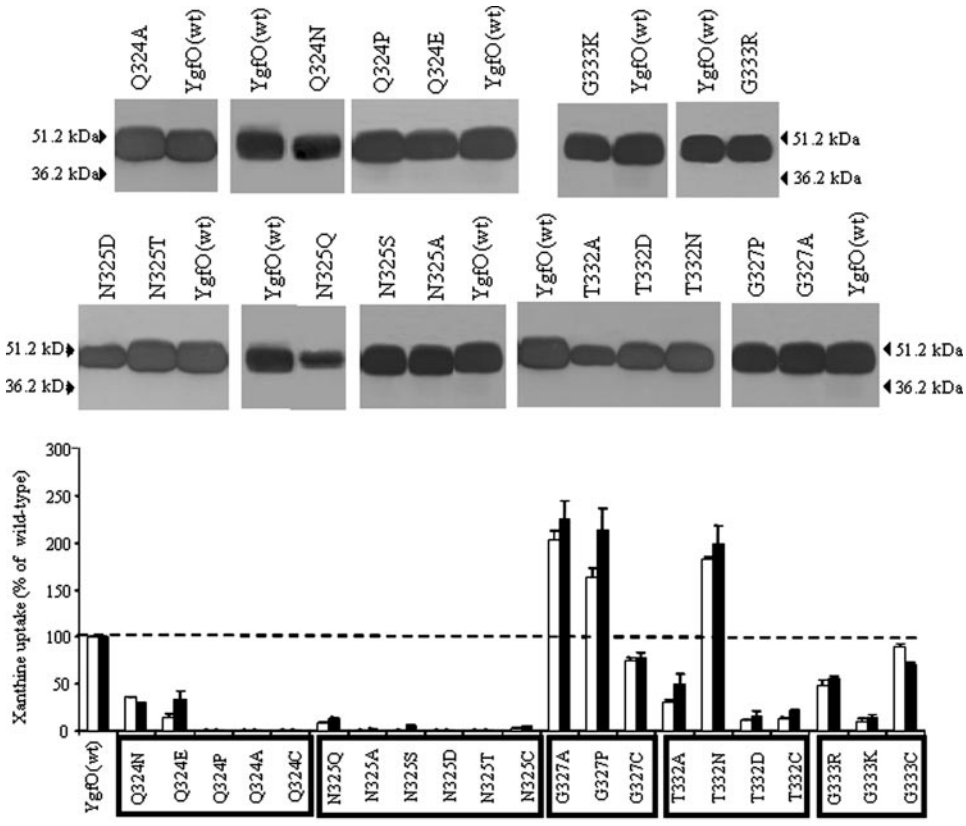

FIGURE 5. **Expression and xanthine uptake activities of site-directed mutants at key conserved residues of the NAT motif.** *E. coli* T184 harboring pT7-5/*ygfO*(wild-type-BAD) with given mutations were grown, induced, and subjected to immunoblot analysis of membrane fractions (*upper panels*) or assayed for transport of [^{3}H]xanthine (1 μM, 25 °C) (*lower panel*) exactly as described in the legends to Figs. 2 and 3. *Open* and *closed histogram bars* represent initial rate and steady state values, respectively.

G340A(wt) is also linked to low expression; all other mutants of this set express normally (Fig. 4*A*).

Transport Analysis of Site-directed Mutants at Conserved Positions of the NAT Motif—The conserved NAT-motif positions Gln-324, Asn-325, and Thr-332, where mutants with negligible or strikingly low activity had been detected (Figs. 2 and 4) as well as the remaining two positions of conserved NAT-motif residues (Gly-327 and Gly-333) were further subjected to extensive site-directed mutagenesis in the wild-type YgfO background. Site-directed mutants were initially analyzed for active xanthine transport (Fig. 5) and kinetics of xanthine uptake (Table 1). Our data show that replacement of Gln-324 with Asn or Glu results in very low levels of accumulation; kinetic analysis reveals that these mutants transport xanthine with high V_{max} but a very low affinity, as reflected by a 15-fold increase in K_m relative to wild-type. Replacement of Gln-324 with Pro, Ala, or Cys results in negligible uptake activity in any of the xanthine concentrations tested. Replacement of Asn-325 with Asp, Gln, Ser, Thr, Cys, or Ala was also found to result in negligible xanthine uptake activity in any of the concentrations tested. In contrast, replacement of Gly-327 with Ala, Pro, or Cys resulted in very high xanthine uptake; that is, 200, 150, or 100% relative to wild type, respectively, and a 2–5-fold increase in V_{max} with a slightly lower K_m. Replacement of Thr-332 with Asn resulted in higher activity than wild type, with a 2-fold lower K_m and an 1.6-fold increased V_{max} but replacement with Asp, Ala, or Cys yielded low activity (Table 1). Finally, although replacement of Gly-333 with Cys resulted in a transport rate and level that was comparable with the ones of wild-type YgfO, replacement with Arg or Lys resulted in low but significant activity; that is, 40–50% that of wild-type for G333R or 10–20% for G333K. In addition, these mutants display V_{max} values that are 2.5- or 5.5-fold lower relative to wild type (Table 1).

Ligand Recognition Profiles of Site-directed Mutants at the NAT Motif—To understand the contribution of selected residues of the NAT motif to the substrate and ligand recognition profile of YgfO, we assayed mutants at positions 324, 327, 332, and 333 for inhibition of [^{3}H]xanthine uptake in the presence or absence of a series of purines and synthetic analogues (Table 2). Mutants Q324N(wt) and Q324E(wt) display an impaired ability for recognition of any of the analogues tested, consistent with their very low affinity for xanthine, as revealed from the kinetics experiments (Tables 1 and 2). In contrast, N325Q(wt) or other mutants at position 325 could not be tested because of negligible activity (Table 1). No major differences in ligand profile were evident for mutants G327A(wt) or G327P(wt), whereas significant changes were observed with both T332N(wt) and T332A(wt) (Table 2). T332N(wt), in particular, displays higher affinity (lower K_i) for 2-thioxanthine (>2-fold), 3-methylxanthine (12-fold), and 8-methylxanthine (>7-fold) and lower affinity (higher K_i) for 1-methylxanthine (13-fold) and 6-thioxanthine (3-fold) (Table 3). Strikingly, important but distinct changes in specificity were observed with mutant G333R(wt). Kinetic analysis of the transport inhibition data for this mutant showed a marginally detectable ability for recognizing uric acid, a 3-fold increase in K_i for 6-thioxanthine, and highly significant decreases in K_i for 8-methylxanthine (4-fold), 3-methylxanthine (5-fold), and 7-methylxanthine (>15-fold) (Table 3). In summary, of the five key conserved residues of the NAT motif, ^{324}**QNNG**VIQM**TG**^{333}, it appears that Gln-324 is critical for high affinity uptake and ligand recognition, Asn-325 is fully irreplaceable with respect to active xanthine transport, and Gly-327 is not mandatory for either active xanthine transport or specificity, whereas Thr-332 and Gly-333 are important determinants of the ligand specificity profile.

Effect of N-Ethylmaleimide on Transport Activity—The effect of NEM, a membrane-permeable sulfhydryl reagent, on the initial rate of xanthine transport for each single-Cys mutant is presented in Fig. 6. When incubated with 2 mM NEM (Fig. 6*A*), it is found that single-Cys at positions 322–329, 332–334, 336, and 339 were inhibited by >80%, T321C was inhibited by 60%, and the activity of the remaining single-Cys mutants was not altered significantly (<1.6-fold enhancement or inhibition). All NEM-inhibitable mutants were then assayed in the concentration range of 5 μM to 2 mM, and the concentration resulting in 50% reduction of initial rate (IC_{50}) was determined (Fig. 6*B*). It is evident that sequence 315–340 can be divided to three consecutive regions of distinct sensitivity; single-Cys positions 315–322 were insensitive to NEM, with IC_{50} values ≥0.4 mM, positions 323–329 were highly sensitive, with IC_{50} values of 15–80 μM, and positions 330–340 followed a pattern indicative of an α-helical conformation, with mutants sensitive to alkylation clustering on one face of an α-helix (Fig. 7).

Alkylation Analysis of the Single-Cys Mutants—Site-directed sulfhydryl alkylation assay using extensive NEM treatment (1 mM, 10 min) was performed for T184 expressing each single-Cys mutant in the sequence 315–340. It is found that all single-Cys positions in this sequence region are highly accessible and reactive with NEM (Fig. 8).

TABLE 1

K_m and V_{max} values of YgfO mutants for xanthine uptake

E. coli T184 expressing the corresponding constructs were assayed for initial rates of xanthine uptake at 5–20 s in the concentration range of 0.1–100 μM; negative control values obtained from T184 harboring vector pT7-5 alone were subtracted from the sample measurements in all cases. Kinetic parameters were determined from non-linear regression fitting to the Michaelis-Menten equation using *Prism*4; values represent the means of three independent determinations with S.D. shown. All mutants as well as the wild-type (wt) and Cys-less YgfO versions used in these experiments contained a C-terminal BAD. ND, assays were performed but kinetic values were not determined due to very low uptake rates.

Permease	K_m	V_{max}	V_{max}/K_m
	μM	*nmol min^{-1} mg^{-1} protein*	μl min^{-1} mg^{-1}
YgfO(wt)	4.6 ± 0.3	6.4 ± 0.5	1391
YgfO(Cys-less)	5.5 ± 0.5	10.2 ± 0.8	1854
Q324N(wt)	76.0 ± 19.1	44.5 ± 4.7	586
Q324E(wt)	71.2 ± 12.2	12.6 ± 0.4	177
N325Q(wt)	ND	ND	
N325C	ND	ND	
G327A(wt)	3.4 ± 0.3	28.9 ± 6.6	8500
G327P(wt)	3.9 ± 0.1	28.1 ± 4.0	7205
G327C	3.2 ± 0.2	20.1 ± 5.1	6281
T332N(wt)	2.2 ± 0.3	10.5 ± 2.2	4772
T332D(wt)	1.7 ± 0.1	0.9 ± 0.1	529
T332A(wt)	4.8 ± 1.2	1.9 ± 0.4	396
T332C	3.0 ± 0.1	1.0 ± 0.1	333
G333R(wt)	2.8 ± 0.3	2.4 ± 0.2	857
G333K(wt)	5.2 ± 1.2	1.1 ± 0.1	211

TABLE 2

Specificity profile of YgfO mutants at conserved residues of the NAT motif

Values shown express % of [^{3}H]xanthine (1 μM) uptake rate in the presence of 1000-fold excess (1 mM) of unlabeled competitors. The uptake value obtained in the absence of competitor was taken as 100%. Values represent the means of at least three determinations; S.D. were always <20%. Most significant differences from the wild-type (wt) profile are highlighted in bold. All mutants as well as the wild-type version used in these experiments contained a C-terminal BAD.

Competitor	[^{3}H]xanthine uptake rate retained							
	wt	Q324N	Q324E	G327A	G327P	T332N	T332A	G333R
					%			
—	100	100	100	100	100	100	100	100
Xanthine	1	0	0	1	1	2	1	2
Uric acid	97	143	122	82	87	73	68	**54**
Hypoxanthine	96	125	90	106	93	85	80	71
Adenine	96	90	124	113	100	110	132	78
Guanine	94	97	80	77	92	68	78	97
Uracil	101	128	98	104	92	81	75	101
1-Methylxanthine	19	**90**	**93**	23	33	5	9	5
2-Thioxanthine	13	**123**	**113**	8	10	**3**	**1**	10
3-Methylxanthine	25	**79**	**85**	18	28	**2**	**3**	**0**
6-Thioxanthine	20	**61**	**50**	**1**	**1**	**1**	**1**	10
7-Methylxanthine	105	69	112	72	89	65	76	**21**
8-Methylxanthine	96	70	75	42	52	**33**	**30**	**18**
9-Methylxanthine	13	**117**	**92**	6	7	**2**	**1**	7
Allopurinol	106	105	124	83	99	65	70	61
Oxypurinol	31	**69**	**62**	8	9	**4**	**1**	10

TABLE 3

Kinetics and specificity profile of YgfO mutants G333R(wt) and T332N(wt)

Most significant differences from YgfO(wt) are highlighted in bold. Competition assay and kinetic analysis were performed as described under "Experimental Procedures." Values with S.D. shown represent the means of three determinations. Untagged versions of YgfO(wt) and G333R(wt) were used in these experiments. ND, not determined.

Unlabeled competitor (1 mM)	[^{3}H]xanthine uptake rate retained		
	YgfO(wt)	G333R(wt)	T332N(wt)
		%	
—	100 ± 4	100 ± 2	100 ± 2
Xanthine	1 ± 2	0 ± 1	2 ± 1
Uric acid	92 ± 2	**49 ± 2**	73 ± 10
Hypoxanthine	91 ± 1	94 ± 2	85 ± 5
Adenine	88 ± 2	108 ± 8	110 ± 6
Guanine	63 ± 5	72 ± 5	68 ± 9
Uracil	97 ± 3	72 ± 1	81 ± 10
1-Methylxanthine	6 ± 1	6 ± 2	5 ± 1
2-Thioxanthine	14 ± 1	16 ± 3	3 ± 1
2-Thiouric acid	18 ± 2	9 ± 1	ND
3-Methylxanthine	16 ± 3	**0 ± 1**	**2** ± 1
6-Thioxanthine	11 + 1	16 ± 3	1 ± 0
7-Methylxanthine	116 ± 2	**18 ± 1**	65 ± 11
8-Methylxanthine	110 ± 8	**13 ± 3**	**36 ± 6**
8-Thiouric acid	7 ± 2	9 ± 2	ND
8-Azaxanthine	72 ± 2	59 ± 6	ND
9-Methylxanthine	6 ± 1	12 ± 4	2 ± 1
		K_i	
		μM	
Uric acid	>1500	**737**	>1500
1-Methylxanthine	36	46	**489**
2-Thioxanthine	91	80	**40**
3-Methylxanthine	72	**14**	**6**
6-Thioxanthine	41	**121**	**112**
7-Methylxanthine	>1500	**107**	>1500
8-Methylxanthine	>1500	**409**	**196**
8-Thiouric acid	57	57	ND
9-Methylxanthine	53	54	36

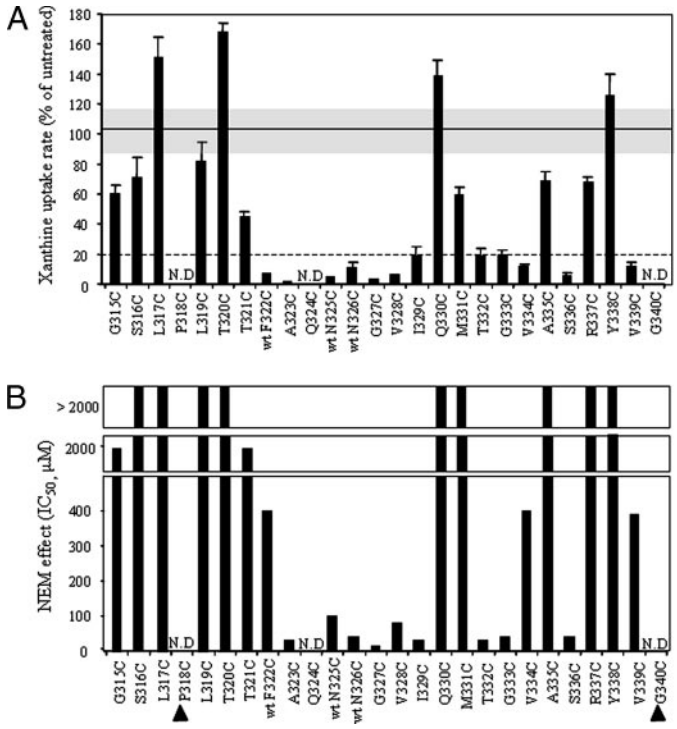

FIGURE 6. **Effect of NEM on the xanthine transport activity of single-Cys mutants.** *E. coli* T184 harboring pT7-5/*ygfO*(C-less-BAD) with given mutations were grown, induced, and assayed for transport of [^{3}H]xanthine (1 μM, 25 °C). Cells had been preincubated in the absence or presence of either 2 mM NEM (*A*) or a range of NEM concentrations (5 μM, 10 μM, 20 μM, 40 μM, 0.1 mM, 0.4 mM, 1 mM) (*B*) for 10 min at 25 °C. Transport assays were performed in the presence of 20 mM potassium ascorbate and 0.2 mM phenazine methosulfate. *A*, effect of 2 mM NEM. Rates are presented as percentages of the rate measured in the absence of NEM with S.D. from three independent determinations shown. Average and S.D. values of C-less control are also shown as a *dashed line* and *gray horizontal bars*, respectively. *B*, NEM concentrations inhibiting activity of each mutant by 50% (IC_{50} values). IC_{50} values were deduced with use of the *Prism*4 software. Values were not determined (*N.D.*) for mutants P318C, Q324C, and G340C, which display negligible initial rates, or determined using Cys-replacements in the wild-type (*wt*) for mutants F332C(wt), N325C(wt), and N326C(wt) (see Fig. 4). Although not shown, transport activity of wild-type YgfO-BAD remained insensitive to the NEM treatment in any of the indicated reagent concentrations.[3] *Solid arrowheads* indicate the positions of mutants P318C and G340C.

DISCUSSION

We have studied the role of the NAT signature motif by Cys-scanning and site-directed mutagenesis in the major xanthine-specific bacterial homolog YgfO. An important first conclusion from this work is that the bacterial NAT motif contains determinants critical for the mechanism of active xanthine transport and purine analogue selectivity. In particular, of the 10-residue sequence considered as the core part of the motif, ^{324}**QN**N**G**VIQM**TG**^{333}, the first two, Gln-324 and Asn-325, are irreplaceable with respect to active xanthine transport, whereas the last two, Thr-332 and Gly-333, play crucial roles with respect to specificity against different analogues. The fifth conserved residue of the NAT motif, Gly-327, does not seem to play a major role in the mechanism with respect to specificity, but replacement of Gly with Ala, Pro, or Cys enhances transport capacity. Strikingly similar observations have been made to a certain extent in a recent mutational study of the NAT motif in the fungal uric acid/xanthine transporter UapA (8). Taken together and compared with the UapA data, our site-directed analyses of YgfO reinforce the importance of Gln-324 (a residue conserved in purine-transporting NAT members) and Asn-325 (a residue conserved throughout the family) as residues absolutely essential for NAT activity and delineate Thr-332 (a residue conserved throughout the family) and Gly-333/Arg (conserved in xanthine-monospecific and uric acid/xanthine dual-specificity NAT types, respectively) as residues playing a fine role in determining NAT specificity. With respect to Gly-327 (a residue that is also conserved throughout the family), it appears that it is not crucial in the xanthine-specific YgfO (11) but becomes most important in determining kinetics and specificity in the uric acid/xanthine-specific UapA (8) probably because the local flexibility conferred by Gly-327 in the putative short loop QNNG is needed for optimal recognition of uric acid or for other UapA-related binding interactions (8).

With respect to the irreplaceable residues of the motif, Gln-324 is mandatory for high affinity uptake of xanthine and recognition of ligands, whereas Asn-325 is fully irreplaceable with respect to active xanthine transport. Regarding Gln-324, replacements yielded normal permease expression but very low (Glu, Asn) or negligible activity (Pro, Ala, or Cys). The detectably active mutants Q324N and Q324E had very low affinity for transport of xanthine (15-fold higher K_m than wild type) and impaired binding affinity for any substrate analogue. These data clearly suggest that high affinity binding of the purine substrate requires both the presence and correct geometry of a carbonyl group at position 324 of YgfO. Analogous data had been obtained previously with the corresponding mutants Q408N,

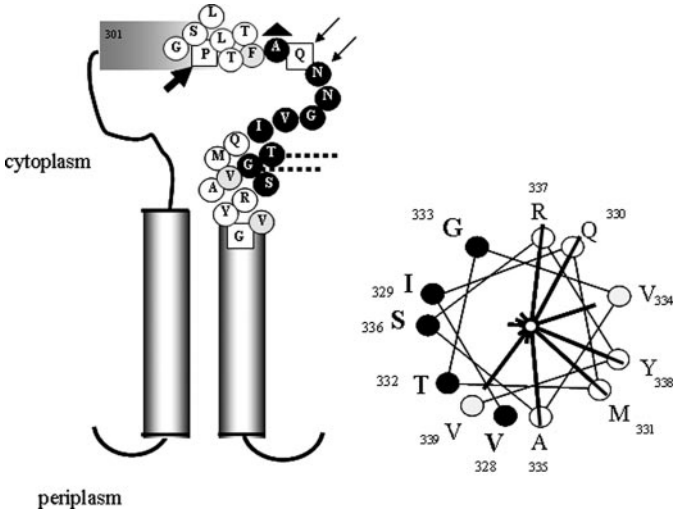

FIGURE 7. **Secondary structure model of the NAT motif and flanking regions of YgfO permease (*left*) and α-helical wheel plot of residues 328–339 (*right*).** Lines radiating from the center of the α-helical plot are proportional to the IC_{50} (NEM) value of each mutant (see Fig. 6). *Solid black circles* indicate positions highly sensitive to NEM treatment ($IC_{50} < 80$ μM), and *solid gray circles* indicate positions of intermediate sensitivity (IC_{50} about 0.4 mM). *Open circles* indicate NEM-insensitive positions ($IC_{50} \geq 2$ mM). *Open squares* indicate positions of negligible single-Cys activity. *Arrows* indicate residues irreplaceable for expression (Pro-318) or activity (Gln-324, Asn-325), and *dashed lines* indicate residues affecting purine selectivity (Thr-332, Gly-333) (see text for details). A cap on top of Ala-323 indicates that NEM sensitivity of mutant A323C is enhanced in the presence of xanthine substrate.[3]

Q408A, Q408P, and Q408S in UapA (8). However, a striking exception was mutant Q408E (7, 8) that appears to bind, but not to transport, the novel, non-physiological NAT substrates hypoxanthine, guanine, and 7-deazaxanthine. Based on the structures of these three purines and the apparent importance of position N9 for UapA-purine interactions (11), the authors suggested (8) that residue 408 might interact with the imidazole ring in the vicinity of N9-H, and the presence of a non-protonated carboxyl group (Glu-408) might allow a novel hydrogen-bonding interaction of UapA with protonated N9-H. Although similar observations are not reproduced in the bacterial NAT with Glu-324, it is evident that the glutamine residue at position 324 plays a critical and finely tuned role in purine binding in both the bacterial YgfO and the fungal UapA system.

Regarding Asn-325, all YgfO replacements (Asp, Gln, Ser, Thr, Cys, or Ala) yielded high expression but undetectable activity at either 25 or 37 °C in any concentration of xanthine substrate, showing that this is a strictly irreplaceable residue with respect to active transport. These findings differentiate partially from the corresponding results of mutational study in UapA (8), where Asn-409 was found to be irreplaceable for active transport or uric-acid dependent growth at 25 °C but easily replaceable (especially with Gln or Ser but even with Ala), with no dramatic effects on transport affinity, capacity, or purine selectivity at 37 °C. It was suggested that Asn-409 might play a conformational role in transport catalysis of UapA without participating in binding. Our data show that the role of Asn-325 in YgfO is more stringent. To understand this irreplaceable role in detail, analysis of substrate binding under non-energized conditions (26) and of partial translocation reactions (27) is needed. Such studies are under way in our laboratory.[4]

With respect to the residues defining selectivity, introduction of an Arg instead of the native Gly residue at position 333 of YgfO modifies the transporter affinity mostly with respect to positions 7 and 8 of the imidazole ring and confers the ability of recognizing ligands selectively modified at these positions, whereas replacement of Thr at position 332 with Asn has a more widespread effect involving reduced affinity for 1-methylxanthine, increased affinity for 3-methylxanthine and unmodified xanthine, and an ability to recognize 8-methylxanthine. It is interesting to note that both G333R and T332N reverse the key specificity elements differentiating the bacterial YgfO and YicE (10) from their fungal homologs UapA and Xut1 (11), *i.e.* they rescue the inability to bind analogues with bulky substitutions at imidazole position 8 and reverse the order of binding contributions of the pyrimidine positions from N3 > N1 and = O2 > = O6 to N1 > N3 and = O6 > = O2 (Table 3). However, none of the two mutants can confer a decent ability to recognize and/or transport the physiological UapA substrate uric acid. In addition, G333R displays the unprecedented property to bind 7-methylxanthine, an analogue that was refractory for binding by any native bacterial or fungal NAT (10, 11) or mutant thereof to be tested (8, 28). Taken together the findings show that replacement of either Thr-332 or Gly-333 has pleiotropic effects on specificity and argue against a direct effect of these residues on substrate binding. The same contention has been reached (8) for the corresponding UapA residues Thr-416 and Arg-417.

A second important conclusion from our work is that the flanking regions around the motif sequence contain determinants critical for the functional integrity of purine pathway. More specifically, residues Ala-323, Asn-326, Gly-327, Val-328, Ile-329, Thr-332, Gly-333, and Ser-336 were found to tolerate replacement with Cys but undergo strong inhibition (IC_{50} values <50 μM) upon further modification by NEM. The finding that both inhibition-sensitive and -insensitive single-Cys replacements are labeled with NEM under equivalent conditions *in vivo* shows that sensitivity to alkylation reflects severe blocking effects of the maleimidyl adduct and not merely increased reactivity or accessibility to the reagent. An immediate steric hindrance on substrate binding should be excluded since no protection from the NEM effect was found in the presence of saturating concentrations of xanthine substrate.[4] The most plausible interpretation is that these residues are critically involved in the conformational changes of turnover, and covalent attachment of the bulky maleimide might block dynamic interactions needed for completion of the xanthine translocation cycle. Such inhibition-sensitive residues have been shown in other transporters (12, 13) to be mostly located at conformationally active faces of transmembrane helices and line the substrate translocation pathway. By analogy, in the case of YgfO permease, we suggest that part of the xanthine translocation pathway is formed by the alkylation-sensitive face in the first few turns of putative transmembrane helix 9 (Fig. 7). In addi-

[4] E. Georgopoulou, P. Panos, and S. Frillingos, unpublished observations.

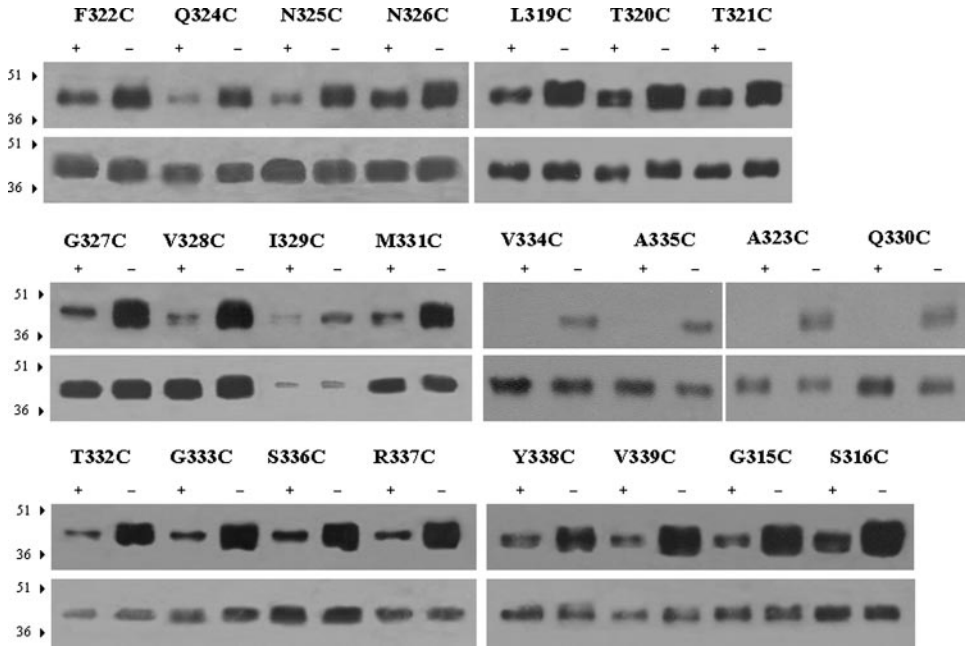

FIGURE 8. **Site-directed NEM labeling of the single-Cys mutants.** *E. coli* T184 expressing His_{10}-tagged versions of given YgfO mutants were incubated in the absence (−) or presence (+) of NEM (1 mM, 10 min) and used to prepare membrane protein extracts and purify the permease by Ni^{2+}-chelate chromatography. Unreacted Cys residues were labeled with OGM (0.2 mM) after denaturation of the Ni^{2+}-captured protein, and OGM-labeled proteins were eluted from the beads by resuspension and brief incubation in Laemmli buffer and analyzed with SDS-PAGE (12%) and immunoblotting using both anti-OGM antibody (*upper blots*) and HRP-conjugated penta-His antibody (*lower blots*). Prestained molecular weight standards (51.2 and 36.2 kDa) are shown on the *left* of each *blot*.

tion, it is clear that the whole region immediately upstream of this helix (323–328), corresponding approximately to the N-half moiety of the NAT motif, plays a primary role in the xanthine translocation mechanism because it contains consecutive residues that are either irreplaceable *per se* (Gln-324 and Asn-325) or subject to irreplaceable constraints in side-chain volume (Ala-323, Asn-326, Gly-327, Val-328). Furthermore, we have found that the NEM reactivity of mutant A323C is greatly enhanced in the presence of xanthine substrate, which strongly supports that this strip of residues is conformationally active and undergoes movements associated with the permease turnover.[4]

Based on *in silico* analyses (8), the first tetrapeptide in the NAT motif (QNNG) appears to form a loop, possibly a turn, between hydrophobic α-helical or β-sheet segments. The Cys-scanning analysis presented herein provides experimental evidence that residues 329–339 immediately downstream of this putative QNNG loop in YgfO form three turns of an α-helix, with residues Ile-329, Thr-332, Gly-333, Ser336, and Val-339 falling on an alkylation-sensitive face that is important for the mechanism of transport (see previous paragraph). Based on these results, we propose that the putative transmembrane helix after the NAT motif, predicted by essentially all available algorithms[5] to run through loop/helix junction Arg-337—Arg-341 to helix/loop junction Ile-356—Ile-363, should extend by at least two additional helical turns within the preceding hydrophilic loop, *i.e.* start from Val-328/Ile-329 (Fig. 7).

[5] TMHMM, HMM-TM, PRED-TMR2, TOPPRED, TMPRED, SOSUI, DAS.

The flanking regions around the motif sequence also appear to contain determinants critical for the structural integrity of the NAT transporter *per se*. More specifically, Pro-318, six residues upstream of the motif, and Gly-340, seven residues downstream, were found to be essential for correct folding and expression in the membrane. It is conceivable that the rigid Pro-318, predicted to be at the kink of a putative α-helical segment preceding the NAT motif sequence (Fig. 1), controls insertion and/or stability of the protein product possibly through dictating architecture of the crucial NAT motif region. Even the presence of a Gly in mutant P318G, allowing flexibility, fails to rescue expression. Inversely, flexibility appears to be required at position 340 of putative transmembrane helix 9, because replacement of Gly-340 even with the small, helix-forming Ala leads to very low expression. Conformational flexibility of Gly residues at transmembrane α-helices (13, 29) or re-entrant loops (30) has been previously linked to efficient substrate binding and transport catalysis in other secondary active transporters.

Overall, the Cys-scanning analysis presented above has demonstrated that the region at and around the NAT motif is a very important site of side-chain determinants with major contributions to the integrity, transport activity, and purine selectivity profile of the transporter. Our ongoing studies are expected to provide a comprehensive general picture for the structure-function relationships of this bacterial NAT model and reveal all important determinants of purine binding, translocation, and specificity.

Acknowledgments—We thank George Diallinas for helpful discussions, H. Ronald Kaback for support and advice, and Sotiria Tavoulari for help with nickel affinity chromatography.

REFERENCES

1. Tsukaguchi, H., Tokui, T., Mackenzie, B., Berger, U. V., Chen, X. Z., Wang, Y., Brubaker, R. F., and Hediger, M. A. (1999) *Nature* **399,** 70–75
2. de Koning, H., and Diallinas, G. (2000) *Mol. Memb. Biol.* **17,** 75–94
3. Liang, W. J., Johnson, D., and Jarvis, S. M. (2001) *Mol. Memb. Biol.* **18,** 87–95
4. Diallinas, G., and Scazzocchio, C. (1989) *Genetics* **122,** 341–350
5. Diallinas, G., Valdez, J., Sophianopoulou, V., Rosa, A., and Scazzocchio, C. (1998) *EMBO J.* **17,** 3827–3837
6. Meintanis, C., Karagouni, A. D., and Diallinas, G. (2000) *Mol. Memb. Biol.* **17,** 47–57
7. Amillis, S., Koukaki, M., and Diallinas, G. (2001) *J. Mol. Biol.* **313,** 765–774
8. Koukaki, M., Vlanti, A., Goudela, S., Pantazopoulou, A., Gioule, H., Tournaviti, S., and Diallinas, G. (2005) *J. Mol. Biol.* **350,** 499–513

9. Vlanti, A., Amillis, S., Koukaki, M., and Diallinas, G. (2006) *J. Mol. Biol.* **357,** 808–819
10. Karatza, P., and Frillingos, S. (2005) *Mol. Memb. Biol.* **22,** 251–261
11. Goudela, S., Karatza, P., Koukaki, M., Frillingos, S., and Diallinas, G. (2005) *Mol. Memb. Biol.* **22,** 263–275
12. Frillingos, S., Sahin-Tóth, M., Wu, J., and Kaback, H. R. (1998) *FASEB J.* **12,** 1281–1299
13. Tamura, N., Konishi, S., Iwaki, S., Kimura-Someya, N., Nada, S., and Yamaguchi, A. (2001) *J. Biol. Chem.* **276,** 20330–20339
14. Wilson, G., and Karlin, A. (2001) *Proc. Natl. Acad. Sci. U. S. A.* **98,** 1241–1248
15. Abramson, J., Smirnova, I., Kasho, V., Verner, G., Kaback, H. R., and Iwata, S. (2003) *Science* **301,** 610–615
16. Mueckler, M., and Makepeace, C. (2005) *J. Biol. Chem.* **280,** 39562–39568
17. Schrodt, S., Koch, J., and Tampe, R. (2006) *J. Biol. Chem.* **281,** 6455–6462
18. Cui, L., Aleksandrov, L., Hu, Y.-X., Gentzsch, M., Chen, J.-H., Riordan, J. R., and Aleksandrov, A. A. (2006) *J. Physiol.* **572,** 347–358
19. Inoue, H., Nojima, H., and Okayama, H. (1990) *Gene* **96,** 23–28
20. Teather, R. M., Bramhill, J., Riede, I., Wright, J. K., Furst, M., Aichele, G., Wilhelm, V., and Overath, P. (1980) *Eur. J. Biochem.* **108,** 223–231
21. Smirnova, I., and Kaback, H. R. (2003) *Biochemistry* **42,** 3025–3031
22. Ho, S. N., Hunt, H. D., Horton, R. M., Pullen, J. K., and Pease, L. R. (1989) *Gene* (*Amst.*) **77,** 51–59
23. Frillingos, S., Sahin-Tóth, M., Persson, B., and Kaback, H. R. (1994) *Biochemistry* **33,** 8074–8081
24. Carrasco, N., Herzlinger, D., Mitchell, R., DeChiara, S., Danho, W., Gabriel, T. F., and Kaback, H. R. (1984) *Proc. Natl. Acad. Sci. U. S. A.* **81,** 4672–4676
25. Granseth, E., Daley, D. O., Rapp, M., Melen, K., and von Heijne, G. (2005) *J. Mol. Biol.* **352,** 489–494
26. Sahin-Tóth, M., le Coutre, J., Kharabi, D., le Maire, G., Lee, J. C., and Kaback, H. R. (1999) *Biochemistry* **38,** 813–819
27. Kaback, H. R. (1997) *Proc. Natl. Acad. Sci. U. S. A.* **94,** 5539–5543
28. Pantazopoulou, A., and Diallinas, G. (2006) *Mol. Memb. Biol.* **23,** 337–348
29. Weinglass, A. B., and Kaback, H. R. (1999) *Proc. Natl. Acad. Sci. U. S. A.* **96,** 11178–11182
30. Yernool, D., Boudker, O., Jin, Y., and Gouaux, E. (2004) *Nature* **431,** 811–818
31. Argyrou, E., Sophianopoulou, V., Schultes, N., and Diallinas, G. (2001) *Plant Cell* **13,** 953–964